ACSNANO

www.acsnano.org

ARTICLE

Pulmonary Delivery of Specialized Pro-Resolving Mediators-Based Nanotherapeutics Attenuates Pulmonary Fibrosis in Preclinical Animal Models

Jiulong Li, Yu Xiao, Yumo Zhang, Silu Li, Minzhi Zhao, Tian Xia,* and Huan Meng*

Cite This: https://doi.org/10.1021/acsnano.2c10388

Read Online

ACCESS | Metrics & More | Article Recommendations | Supporting Information

Downloaded via NATL CTR NANOSCIENCE & TECHNOLOGY on August 8, 2023 at 03:20:54 (UTC).
See https://pubs.acs.org/sharingguidelines for options on how to legitimately share published articles.

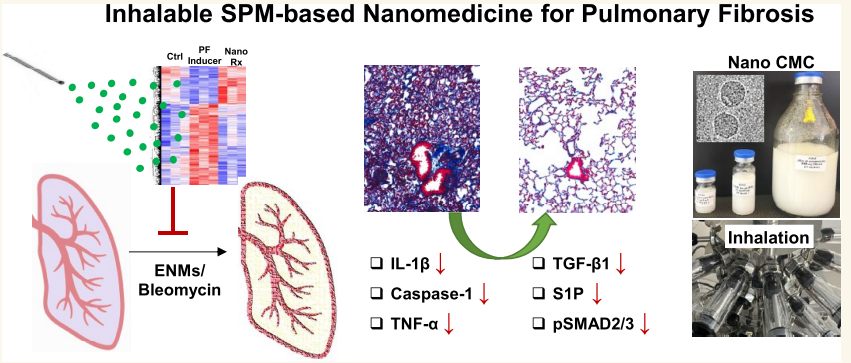

ABSTRACT: **Pulmonary fibrosis (PF) is a chronic lung disease characterized by excess extracellular matrix deposition and prolonged inflammation that fails to resolve and is druggable. Using resolvins and their precursors for inflammation resolution, we demonstrate a nano-enabled approach for accomplishing robust antifibrotic effects in bleomycin- or engineered nanomaterial-induced mouse and rat PF models. Targeting the lipid peroxidation-triggered NLRP3 inflammasome and NF-κB pathway in macrophages and the ROS-mediated TGF-β/Smad and S1P signaling in epithelial cells results in these potent protective effects at the ng/mL dosimetry. We further develop an inhalable biocompatible nanoparticle that encapsulates fish oil, a chosen resolvin precursor, with phosphatidylcholine and polyethylene glycol to enhance drug permeability and facilitate crossing the mucosal barrier, forming "*fish-oilsome*" (FOS). Oropharyngeal aspiration and inhalation of FOS improved the anti-inflammatory status, histological characteristics, and pulmonary function in fibrotic lungs, which was mechanistically supported by transcriptomic and proteomic analyses. Further, scale-up engineered FOS samples with the desired physicochemical properties, anti-PF efficacy, and *in vivo* biocompatibility were validated in different batch sizes (up to 0.2 L/batch). This study provides a practical and translatable approach to promoting inflammation resolution and PF treatment.**

KEYWORDS: *pulmonary fibrosis, specialized pro-resolving mediators, pulmonary drug delivery, inflammation resolution, nanomedicine*

INTRODUCTION

Pulmonary fibrosis (PF) is a serious lung disease involving many different risk factors, including exposure to chemicals, particles, and fibers or reaction to certain medications such as bleomycin (BLM).[1−3] PF is characterized by chronic inflammation and accompanied by excessive deposition of the extracellular matrix that causes progressive scarring or thickening of tissues between the lung's alveoli, leading to reduced pulmonary functions and eventually respiratory failure.[4,5] Recently, PF has been identified in 56% or 71% of the patients who experienced moderate or severe COVID-19.[6,7] Nintedanib and pirfenidone are the major medications for PF; however, they are costly with significant side

Received: October 19, 2022
Accepted: July 26, 2023

© XXXX American Chemical Society

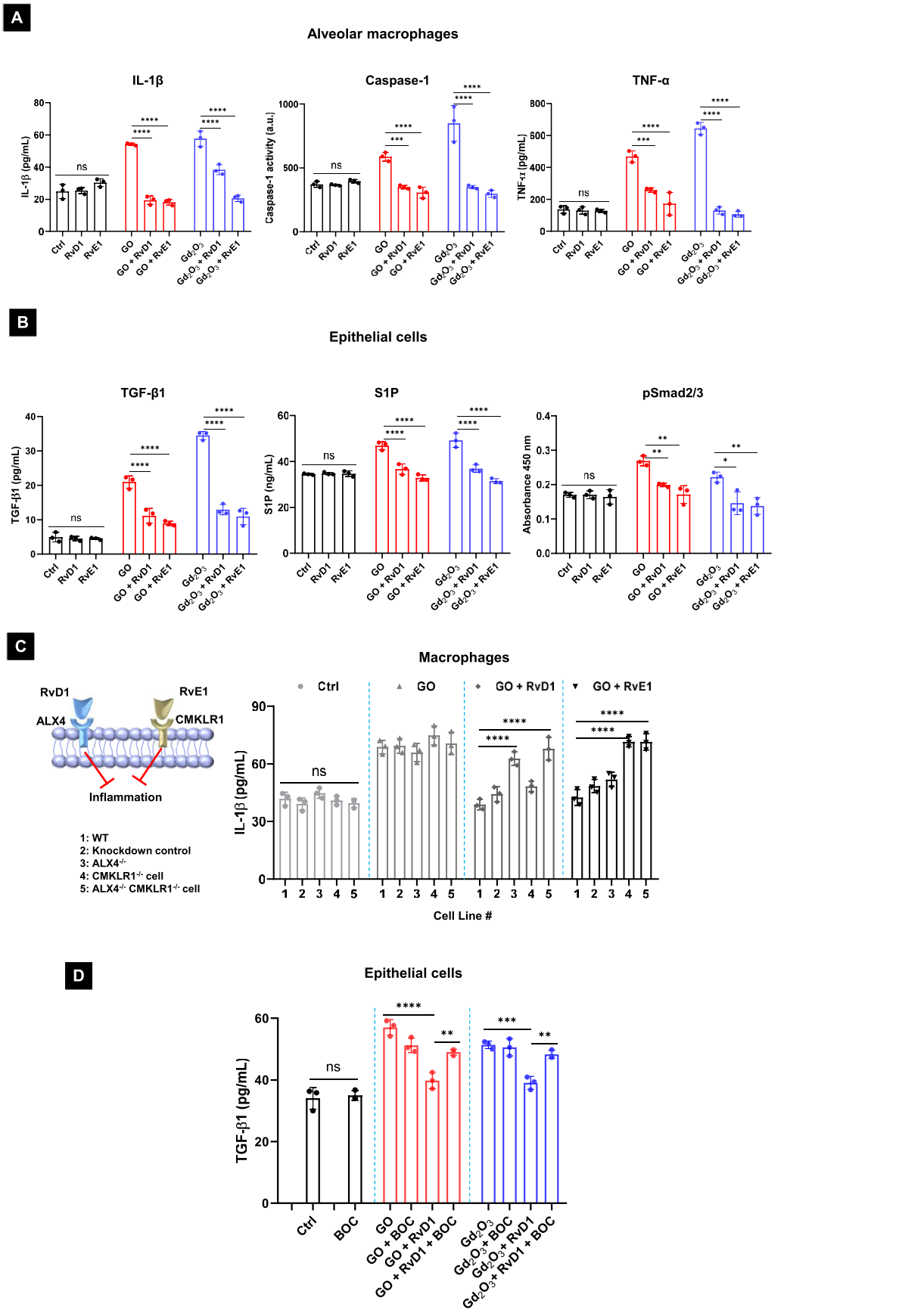

Figure 1. Effective anti-inflammatory and antifibrogenic effects of resolvins in macrophages and epithelial cells. (A, B) RvD1 and RvE1 effects on GO or Gd_2O_3 nanoparticles-induced IL-1β release, caspase-1 activation, and TNF-α production in alveolar macrophages (A), as well as TGF-β1 release, S1P production, and Smad2/3 phosphorylation in epithelial cells (B). (C, D) Demonstration of receptor-specific resolvin effect

https://doi.org/10.1021/acsnano.2c10388
ACS Nano XXXX, XXX, XXX−XXX

Figure 1. continued

using siRNA or pharmacological inhibitor. In macrophages, the effectiveness of RvD1 was interfered in ALX4$^{-/-}$ (siRNA knockdown RvD1 receptor) and double-negative (ALX4$^{-/-}$ CMKLR1$^{-/-}$) cells, while the RvE1 effect was sensitive to CMKLR1$^{-/-}$ (siRNA knockdown RvE1 receptor) or double-negative knockdown macrophages (C). An RvD1 receptor antagonist, BOC-2, abolished the inhibition effect of RvD1 on ENMs-induced TGF-β1 production in epithelial cells (D). Graphs show the mean ± SEM. Data are representative of at least two independent experiments and analyzed using a two-tailed Student's *t* test. *$p < 0.05$, **$p < 0.01$, ***$p < 0.001$, ****$p < 0.0001$, and "ns" indicates no significance.

effects and limited therapeutic efficacies.[4,5,8] It is urgently needed to develop emerging pharmacological strategies for PF treatment. Since the presence of chronic inflammation that fails to resolve is a hallmark of PF,[9,10] effective control of inflammation would ameliorate disease severity.

The inhibition or cessation of inflammation, named "inflammation resolution", has been demonstrated to be an active process to promote the return to homeostasis,[11−13] which functionally relies on specialized pro-resolving mediators (SPMs). The SPM family has ∼47 identified single members and mainly includes docosahexaenoic acid (DHA)-derived D-series resolvins (RvDs, such as RvD1) and the eicosapentaenoic acid (EPA)-derived E-series resolvins (RvEs, such as RvE1).[14−17] Previous preclinical studies have demonstrated both the anti-inflammatory and pro-resolving capabilities of SPMs in acute and chronic diseases, such as acute lung injury, inflammatory diseases, persistent pathological pain, and cancers.[18−23] While frequently tested in animals and recently in humans, the mechanism of SPM is not fully understood yet.[18,21−23] Moreover, there is a major hurdle in the delivery of SPMs due to their hydrophobicity, instability, and short half-lives for applications *in vivo*.

In addition to the capability of deep lung penetration, we envisage the use of nanocarriers to implement SPM biology for PF management. We begin our study by demonstrating the highly potent antifibrotic effects of resolvins, in the recently developed engineered nanomaterials (ENMs)-induced PF models, at cellular and intact animal levels. The reason that ENMs-induced PF models are first used is that the emerging occupational hazardous materials, ENMs, generate inflammasome activation and reactive oxygen species (ROS) production that resolvins target.[24,25] The ENMs data further encouraged us to expand the scope of our work such as using resolvin-based therapy to treat PF induced by both BLM (a classic PF inducer) and ENMs in mice and rats. By focusing on the lipid peroxidation-triggered NLRP3 inflammasome and NF-κB pathways in macrophages and the ROS-mediated TGF-β/Smad and S1P signaling in epithelial cells in a receptor-dependent manner, which has not been previously reported, we demonstrated the viability of achieving the elimination of inflammatory or fibrogenic responses using RvD1 or RvE1 at a ng/mL dose. This has prompted us to develop an inhalable biocompatible lipid-based nanoparticle, using chosen resolvin precursors originating from an FDA-approved excipient, fish oil, with phosphatidylcholine and polyethylene glycol to enhance drug permeability through the lung epithelium and facilitate crossing the mucosal barrier and improve resolvin bioavailability. This choice is advantageous in terms of the ease of formulation, cost-effectiveness, FDA readiness of fish oil, and particle stability. Moreover, the successful demonstration of fish oil nanoparticles in treating PF would provide the basis for the iterative design of our formulation capable of the endogenous transformation of resolvins and other SPMs. Oropharyngeal aspiration and inhalation of the resulting nanoformulation, *fish*-oilsome or FOS for short, led to efficient biodistribution in the lungs; this uptake resulted in markedly reduced PF status and outperformed intraperitoneal and oral administrations. To develop FOS production for robust preclinical work for comparative studies using different PF inducers and various animal models, we established a scale-up synthesis protocol of FOS at different batch sizes, up to 0.2 L/batch. The promising mouse data and availability of a bigger FOS batch encouraged us to expand the scope of our investigation to treat rats (∼200 g body weight) that received ENMs or BLM and monitor lung function in live animals, in addition to the histological and biochemical assays. The rat data are not only consistent with the discovery in mice but also allow the generation of comprehensive transcriptomics and proteomics data to elucidate the effects of FOS. Equally important, FOS is highly biocompatible both *in vitro* and *in vivo*.

RESULTS

Resolvins Ameliorate Inflammation and Fibrogenesis in a Receptor-Dependent Manner. Many stimuli including ENM exposure could activate inflammasomes and induce PF in the lungs.[24,25] However, whether SPMs could be used to inhibit ENM-induced PF is an open question. To test the effect of SPMs, the representative 2D nanomaterials such as graphene oxide (GO) and rare earth nanomaterial such as Gd_2O_3 nanoparticles with occupational risk[24−26] were used as inflammation and fibrogenesis inducers in alveolar macrophages or epithelial cells. As shown in Figure S1, the endotoxin-free GO (∼590 nm) and Gd_2O_3 (∼45 nm) nanoparticles induced significant inflammatory responses evidenced by the production of proinflammatory cytokine interleukin-1β (IL-1β) and tumor necrosis factor α (TNF-α) in macrophages. In epithelial cells, ENM exposure triggered the production of transforming growth factor β1 (TGF-β1, a central mediator of fibrogenesis) that is stimulated by sphingosine-1-phosphate (S1P, a signaling sphingolipid). When administrated *in vivo*, GO and Gd_2O_3 yielded an increased level of platelet-derived growth factor-AA (PDGF-AA) in the bronchoalveolar lavage fluid (BALF) and collagen deposition in the lung. The use of RvD1 or RvE1 at 100 ng/mL significantly improved the cell viability in various macrophages (Figure S2) and, more importantly, inhibited inflammatory responses, evidenced by reduced IL-1β release, caspase-1 activation, and TNF-α production to the baseline in the alveolar macrophages (Figure 1A). Similar inflammation resolution effects were obtained in other macrophages, such as KUP5, THP-1, and RAW264.7 cells (Figure S3). Moreover, RvD1 and RvE1 potently reduced the levels of TGF-β1, S1P, and Smad2/3 phosphorylation (regulating TGF-β-responsive gene transcription) to the baseline in the lung epithelial cell line BEAS-2B (Figure 1B), improving the cell viability in this cell type (Figure S4). This suggests the potential protective effects of RvD1 and RvE1 in both macrophages and epithelial cells. Thus, we continued to elucidate the detailed working mechanisms

https://doi.org/10.1021/acsnano.2c10388
ACS Nano XXXX, XXX, XXX−XXX

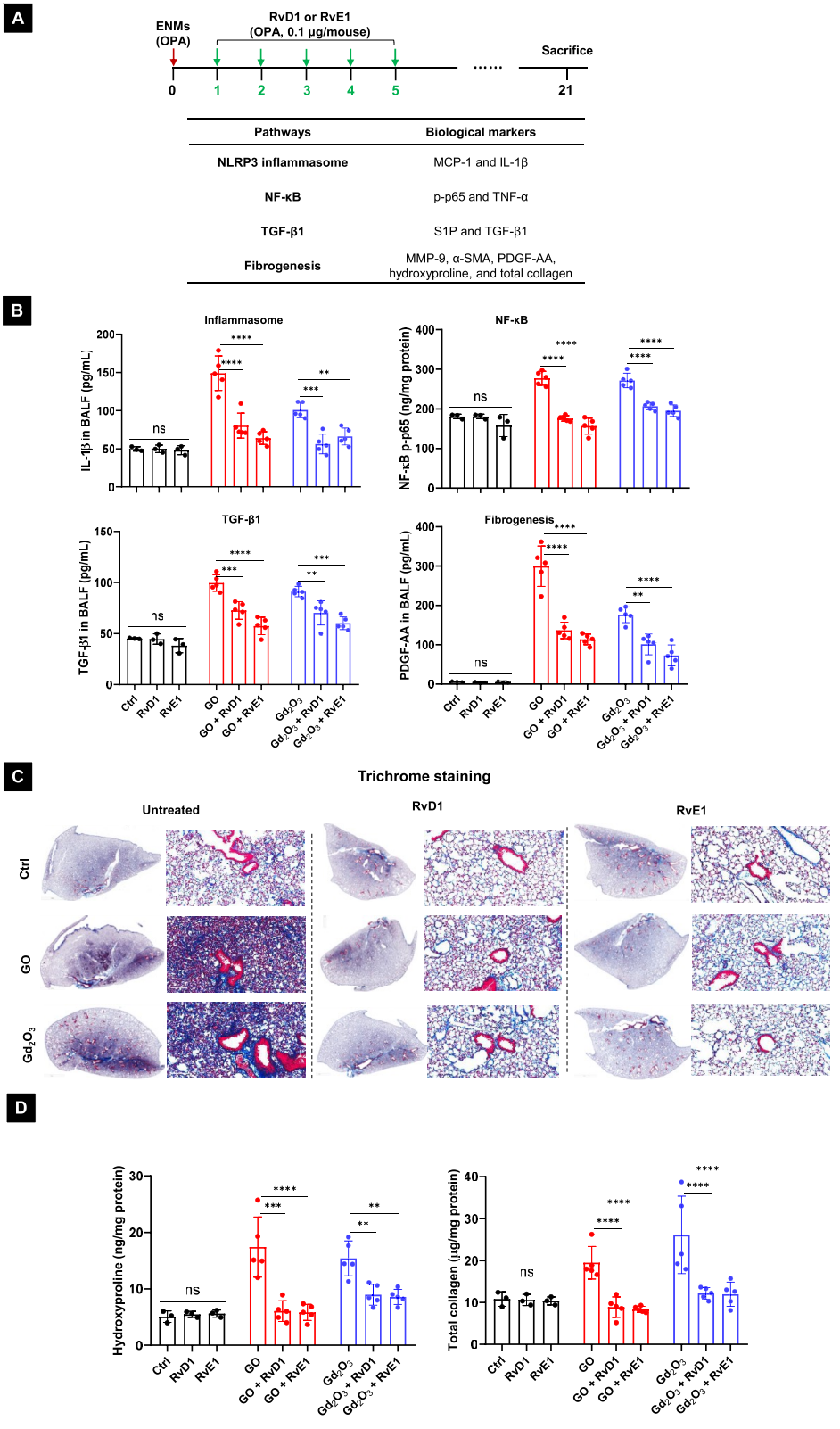

Figure 2. Resolvins lead to inhibited inflammatory and fibrotic responses in ENMs-induced PF models in mice. (A) Schematic illustration of the experimental animal protocol. Eight-week-old C57BL/6 mice received indicated ENMs (2 mg/kg), followed by a total of 5 doses of resolvins (5 μg/kg) through OPA from day 1 to day 5. Animals were sacrificed for tissue harvesting and collection of BALF on day 21 to determine inflammatory responses and fibrotic effects. (B) Major indications to determine the beneficial effects of RvD1 and RvE1 on NLRP3 inflammasome activation, NF-κB pathway, TGF-β1 production, and PDGF-AA abundance in animal lungs or BALF. Additional biochemical markers were also measured (Figure S9). (C) Masson's trichrome staining to demonstrate collagen deposition in the lungs. (D) Hydroxyproline content assay as well as Sircol soluble collagen assay to assess the collagen. Graphs show the mean ± SEM. Data are analyzed using a two-tailed Student's *t* test. *$p < 0.05$, **$p < 0.01$, ***$p < 0.001$, ****$p < 0.0001$, and "ns" indicates no significance.

https://doi.org/10.1021/acsnano.2c10388
ACS Nano XXXX, XXX, XXX−XXX

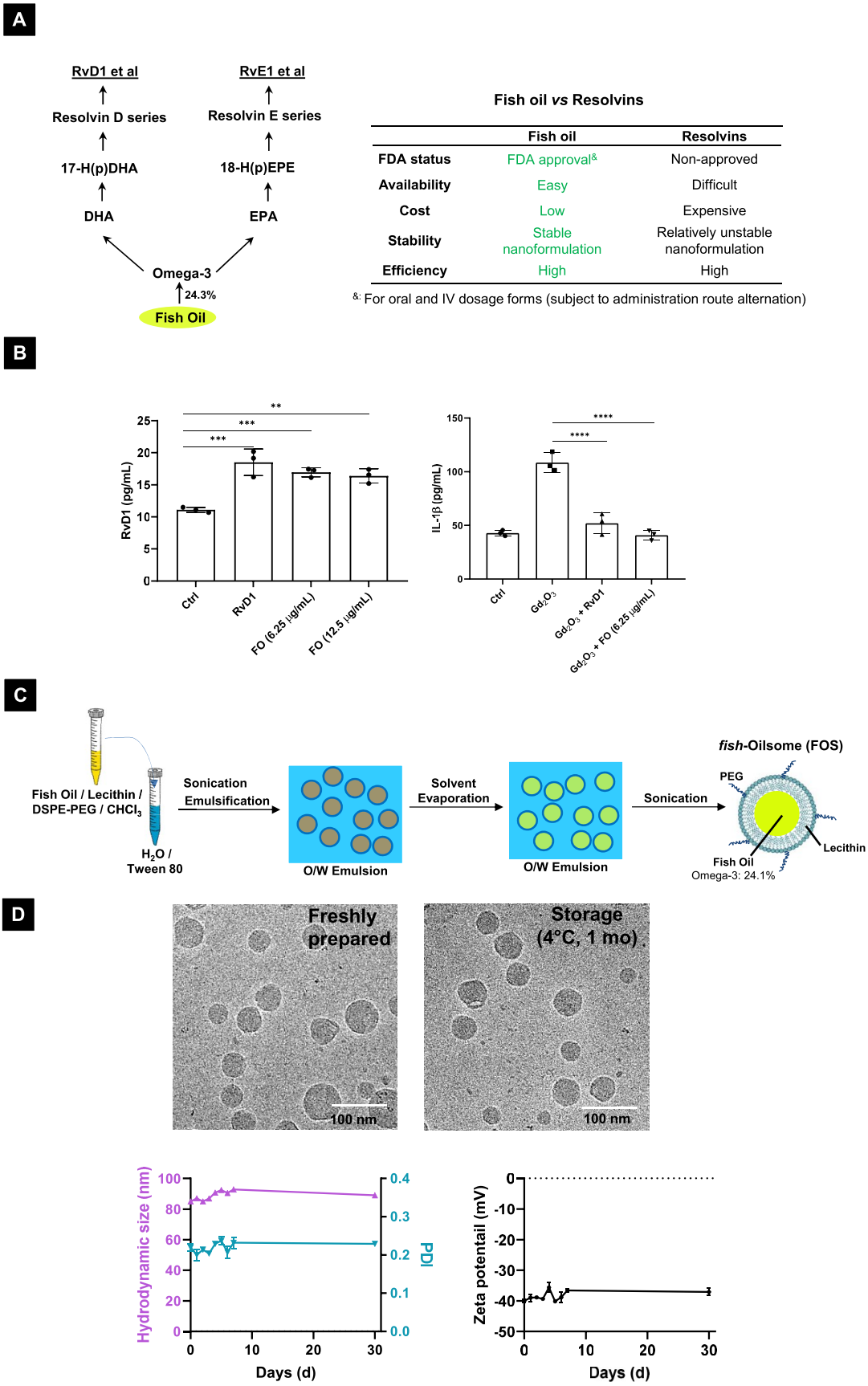

Figure 3. continued

https://doi.org/10.1021/acsnano.2c10388
ACS Nano XXXX, XXX, XXX−XXX

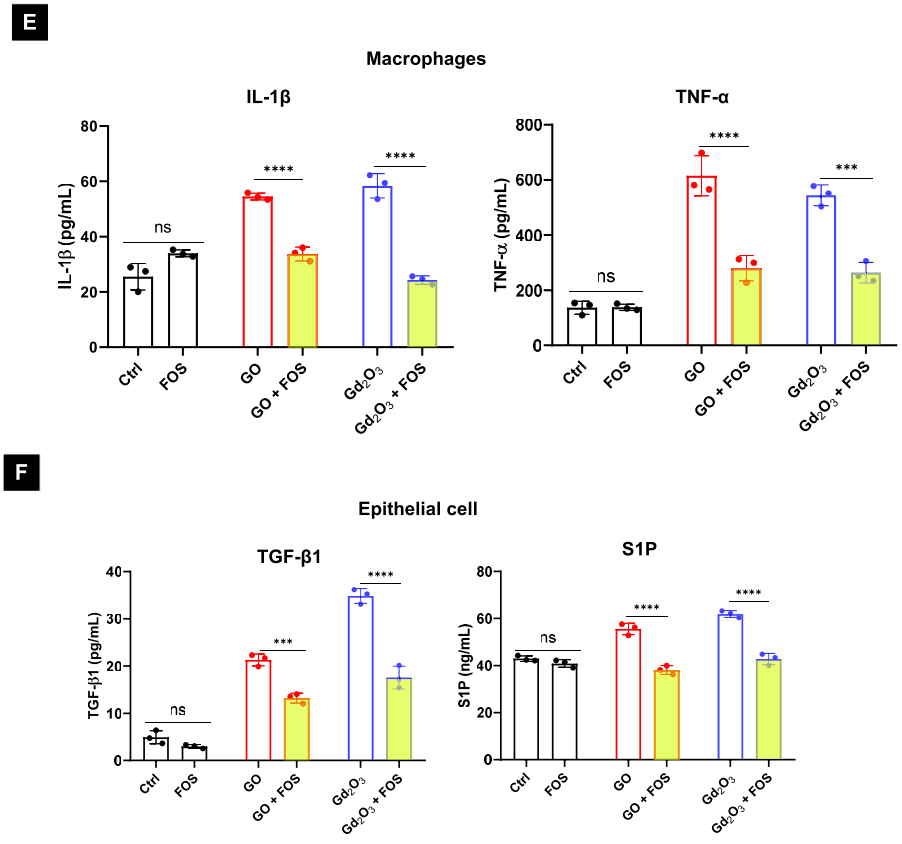

Figure 3. Customized design of a pulmonary nanocarrier for the protective delivery of resolvin precursor (fish oil). (A) Justification of payload choices for designing resolvin-based pulmonary nanotherapy. A simplified scheme to show the endogenous production of resolvin through fish oil (left). Comparative analysis between fish oil and resolvins behooves us to prioritize fish oil as a payload (right). (B) Comparative analysis between adding pure or endogenous produced resolvin (left). Fish oil treatment is functionally equivalent to the pure resolvin treatment (right). (C) Schematic illustration to prepare FOS by a single emulsification/solvent evaporation method. (D) Characterization of FOS morphology, size, zeta potential, and colloidal stability using DLS and cryo-EM. (E, F) Confirmatory cellular study to show the anti-inflammatory and antifibrotic effects in macrophages (E) and epithelial cells (F). FOS, highlighted by the light yellow color, was capable of inhibiting these cellular responses. Graphs show the mean ± SEM. Data are representative of at least two independent experiments and analyzed using a two-tailed Student's *t* test. *$p < 0.05$, **$p < 0.01$, ***$p < 0.001$, ****$p < 0.0001$, and "ns" indicates no significance.

involved in the attenuation of ENMs-induced inflammation and fibrosis.

Resolvins exert their functions by binding to their respective receptors.[15] Through the use of siRNA that targets the RvD1 receptor (ALX4), RvE1 receptor (CMKLR1), or both, we found receptor-dependent inflammation resolution by RvD1 and RvE1 in these knockdown macrophage lines. For example, after GO exposure, the effectiveness of RvD1 was interfered with in ALX4$^{-/-}$ and double-negative (ALX4$^{-/-}$ CMKLR1$^{-/-}$) cells, while the effect of RvE1 was abolished in the CMKLR1$^{-/-}$ or double-negative knockdown macrophages (Figure 1C). We confirmed these findings in the macrophage cell line set, receiving Gd_2O_3 nanoparticles as an inflammation inducer (Figure S5). Unlike Figure 1A, in which we saw RvD1- and RvE1-mediated TNF-α reduction, TNF-α production remained high in the double-negative knockdown cells, irrespective of the RvD1 or RvE1 treatment, indicating the contribution of the resolvin receptor-dependent TNF-α pathway (Figure S6). *In vitro* knockdown efficiency and cell viability checks were conducted to safeguard the data quality during the macrophage knockdown experiment (Figure S7).

Similarly, the resolvin effects on TGF-β1 reduction in epithelial cells could be attributed to the above receptor-specific effects on the TGF-β/Smad signaling pathway.[27] While the ideal scenario is to repeat these experiments in epithelial cells, we ultimately decided to use a pharmacological RvD1 receptor antagonist, *tert*-butyloxycarbonyl 2 (BOC-2), owing to inefficient knockdown effects using siRNA in BEAS-2B cells. As shown in Figure 1D, the pretreatment by BOC-2 significantly attenuated the inhibition effect of RvD1 on ENMs-induced TGF-β1 production, confirming the receptor-dependent TGF-β1 reduction by resolvins. In light of the potential synergy using resolvins in the lung alveolus that involves both macrophage and epithelium, we asked if resolvins could contribute to PF improvement induced by ENMs at the intact animal level.

Resolvins Improve ENMs-Induced Lung Fibrosis in Mice by Inflammation Resolution. To assess the effect of SPMs *in vivo*, we first assessed the effects of RvD1 and RvE1 through oropharyngeal aspiration (OPA) in C57BL/6 mice, which were pretreated by GO or Gd_2O_3 at 2 mg/kg dose according to our pilot study (Figure S1D) and previous reports.[24,25,28] While inhalation administration is the most natural way of exposure, it is technically demanding and expensive and requires special equipment.[25,28] Thus, we decided to conduct the inhalation experiment at the confirmatory stage of biological testing (see below). OPA, however, is a much simpler exposure procedure, which is more robust during the platform iteration stage. After ENM exposure, OPA of 5 μg/kg

https://doi.org/10.1021/acsnano.2c10388
ACS Nano XXXX, XXX, XXX−XXX

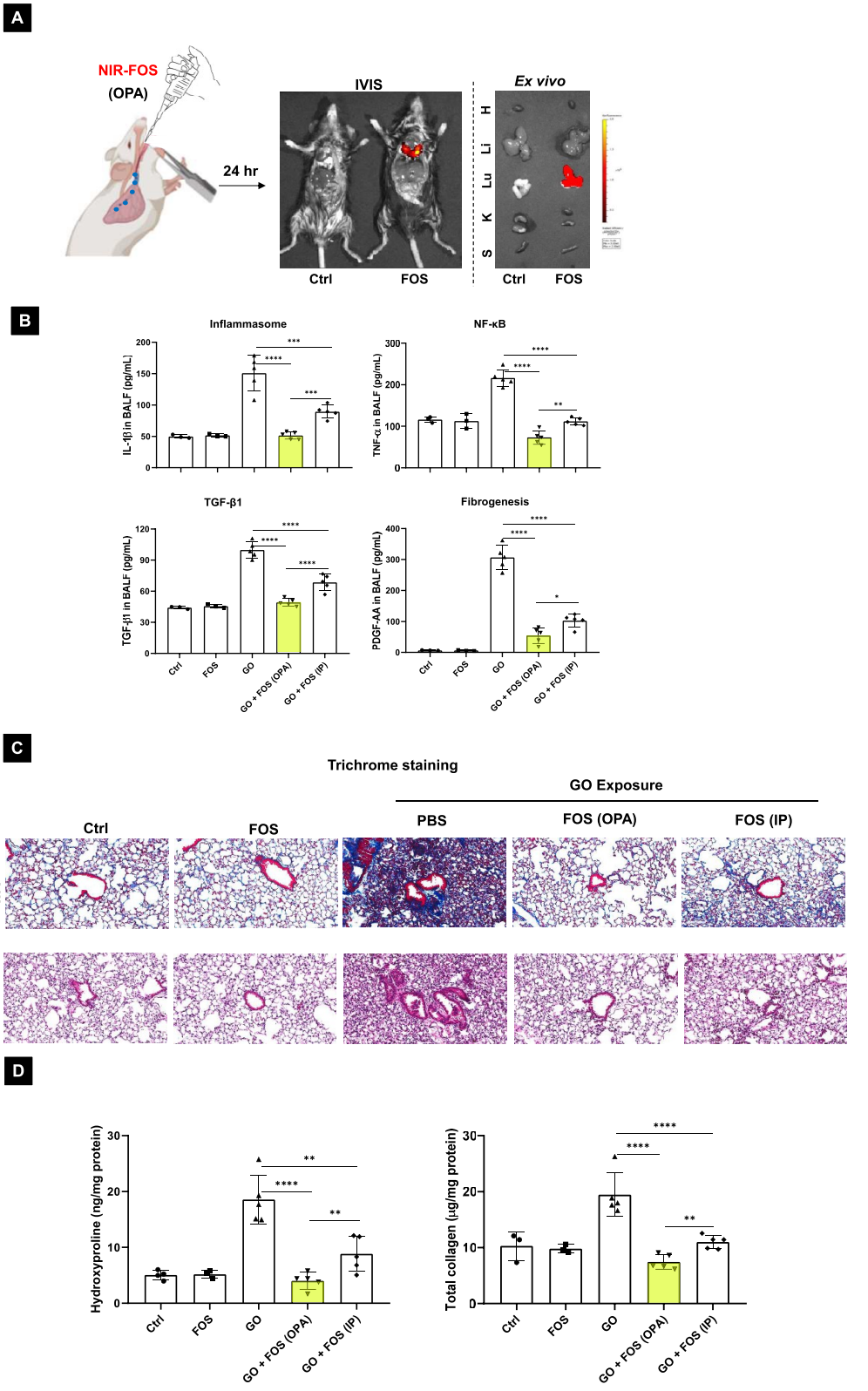

Figure 4. Improved PF status during pulmonary administration of FOS in mice. (A) In the biodistribution study, representative intact animal or *ex vivo* IVIS images were provided to show the delivery efficiency in the lungs after OPA administration of Cy5.5-labeled FOS at 24 h. (B) The FOS efficacy study is similar to Figure 2A. After FOS treatment (2.5 mg/kg, daily for 5 times), NLRP3 inflammasome activation (IL-1β production), NF-κB pathway (TNF-α level), TGF-β1 pathway (TGF-β1 abundance), and fibrogenic effects (PDGF-AA level) were quantified in lungs or BALF. We also compared the effects of OPA vs IP FOS at identical doses, and the former yielded a more efficacious effect in the lungs. (C) MT and H&E staining to determine collagen deposition in the lungs after various treatments. (D) Assessment of the hydroxyproline and total collagen levels in the lung. Graphs show the mean ± SEM. Data are analyzed using a two-tailed Student's *t* test. The confirmatory animal data using inhalation appear online, Figure S21. *$p < 0.05$, **$p < 0.01$, ***$p < 0.001$, and ****$p < 0.0001$.

https://doi.org/10.1021/acsnano.2c10388
ACS Nano XXXX, XXX, XXX−XXX

RvD1 or RvE1 was repeated daily, for a total of 5 administrations, followed by animal sacrifice on day 21 (Figure 2A). In terms of SPM abundance in the BALF, although ENMs significantly depleted SPMs, the exogenous administration of RvD1 or RvE1 efficiently restored the level of SPMs (Figure S8). Biomarkers that involve NLRP3 inflammasome, NF-κB, TGF-β1, and fibrogenesis pathways were measured (Figure 2A). Both RvD1 and RvE1 had a significant inhibitory effect on the ENMs-induced increase in IL-1β, NF-κB p65 phosphorylation (p-p65), TGF-β1, and PDGF-AA (Figure 2B). A similar trend was observed during the measurements of monocyte chemoattractant protein-1 (MCP-1), TNF-α, S1P, matrix metallopeptidase 9 (MMP-9), and α-smooth muscle actin (α-SMA) (Figure S9). Further, collagen deposition and histological features revealed by Masson's trichrome (MT; Figure 2C) and H&E staining (Figure S10) demonstrated a significant decrease in collagen content around small airways under RvD1 or RvE1 treatment. Hydroxyproline, a catabolized form of collagen serving as an indicator of the severity of PF, was significantly reduced after resolvin treatment (Figure 2D, left). The quantitative analysis using the Sircol soluble collagen assay also confirmed the reduced collagen content by RvD1 or RvE1 (Figure 2D, right). Collectively, our data indicate the vital role of RvD1 and RvE1 in improving PF *in vivo*, and the mechanisms could be attributed to the interference of NLRP3 inflammasome activation and the TGF-β/Smad signaling pathway, in line with the results *in vitro*.

Synthesis, Characterization, and Cellular Study of Resolvin Precursor Nanocarrier. While experimentally promising, *in vivo* utilization of resolvins for PF management requires the proper design of a pulmonary delivery system. This is critical because resolvins are hydrophobic, expensive, and subject to rapid degradation with a short biological half-life.[14,29] Our original attempt to obtain resolvin entrapment by a nanoemulsion was met with limited practicability. This is likely due to instability in the stepwise manufacturing procedure and cost restriction, among other factors. We also realize that resolvins are enzymatically derived from omega-3, which is abundantly contained in fish oil.[30−32] Instead of direct resolvin encapsulation, we hypothesized that using fish oil, an FDA-approved substance for intravenous and oral administration capable of endogenous resolvin conversion, could be an easy and inexpensive way to form antifibrosis nanoparticles (Figure 3A).[30−32] Before the formulation study, we also showed a significant increase in RvD1 levels in macrophages under the fish oil treatment (Figure 3B, left); the cellular data further showed that the conversion of fish oil to RvD1 under various fish oil concentrations of 6.25, 9.375, 12.5, and 18.75 μg/mL was calculated to be ~0.25% (Figure S11), which is consistence with the literature.[13,14,18,29−32] Also, the addition of 6.25 μg/mL of fish oil was functionally equivalent to the IL-1β production blockage effect using 100 ng/mL RvD1 in cultured macrophages undergoing inflammation (Figure 3B, right). Subsequently, fish oil nanoparticles (*fish-oilsome*, FOS) were prepared as described in Figure 3C. FOS with a loading efficiency of 94.68 ± 2.03% demonstrated a spherelike structure with an average diameter of 54.18 ± 9.42 nm, a polydispersity index (PDI) of 0.21 ± 0.01, and a zeta potential of −39.00 ± 1.24 mV (Figure 3D). No major changes were observed over 30 days of storage at 4 °C. At the cellular level, FOS improved ENM-induced cell viability (Figure S12) and was capable of blocking IL-1β and TNF-α production in alveolar macrophages (Figure 3E). The inflammation resolution effects were also observed in other macrophage cell lines (Figures S13 and S14). Impressively, FOS also significantly abrogated TGF-β1 and S1P production induced by GO and Gd_2O_3 exposure in BEAS-2B cells (Figure 3F). Furthermore, we found that the protective effects of omega-3-containing FOS cannot be achieved, at the same potency, by other fish oil components, such as DHA, DPA, EPA, and ALA, which were formulated as nanoparticles at a dose of 500 ng/mL (Figure S15). By the combined reasons of potency and the ease-of-formulation, FOS was chosen in this study.

Pulmonary Delivery of FOS Prevents ENMs- and BLM-Induced Fibrogenesis in Mice. Fully characterized and *in vitro* validated FOS was tested in mice. FOS biodistribution to the lung was assessed by a single OPA of 2.5 mg/kg of Cy5.5-labeled FOS (Figure 4A). IVIS imaging of the whole animal and explanted organs was performed in 4 (Figure S16) or 24 h (Figure 4A) after OPA administration. This demonstrated a highly efficient fluorescent intensity enrichment in the lung. By calculating the fluorescent intensity in the lung, we found that about 30−53% of FOS biodistributed in the lungs while the rest presumably could go into the gastrointestinal tract. Also, we found the OPA of 0.05 mg of FOS would bring about 173.53 pg/mL net increase in RvD1 in BALF (Figure S17), which is in agreement with the literature.[13,29−32] Similar to Figure 2A, we repeated the antifibrosis efficacy study using FOS at 2.5 mg/kg, administrated 5 times. In this case, we first utilized GO as the PF inducer and also included FOS only and GO plus intraperitoneally (IP) injected FOS, as additional controls. FOS significantly attenuated the levels of IL-1β, TNF-α, TGF-β, and PDGF-AA in GO-induced PF mice, outperforming all the controls (Figure 4B). A similar trend was observed during the measurement of MCP-1, MMP-9, and α-SMA (Figure S18). These findings were corroborated by MT (Figure 4C) and H&E staining (Figure S19), demonstrating a significant decrease in collagen content around small airways under FOS treatment. Likewise, the quantification of hydroxyproline and collagen analyses (Figure 4D) confirmed the efficacy of FOS. Interestingly, the OPA outperformed IP treatment (Figure 4). In a separate animal experiment, we also compared OPA vs results of oral gavage using the same dose of FOS nanoparticles in the BLM-treated mice to rule out the effect of orally administrated FOS (Figure S20). The efficacy of oral FOS was minimal (Figure S20, fourth column). Therefore, both the IP and oral gavage data demonstrated the advantage and necessity of pulmonary drug delivery to target the resolvin pathway in the lungs. In addition to the experimental administration route using OPA, we further performed an additional efficacy study to treat BLM-induced PF in mice via inhalation. The results in Figure S21 demonstrated that the inhalation exerted significant antifibrogenesis, inflammation resolution, collagen degradation, and lung function improvement outcomes, which confirmed the effectiveness of our nanoparticle in animal lungs using a clinically popular administration route.

Effective Pulmonary Function Restoration and Anti-PF Effects by FOS in Rat Models. In order to fully understand the anti-PF effect *in vivo*, it was necessary to expand the animal species, fibrosis inducer, and PF biological end points. To streamline FOS production for a comprehensive series of comparative studies, i.e., testing multiple PF inducers in rats other than mice, it was necessary to scale up the synthesis of the nanoparticles at different quantities. Until now, we have established protocols for making 75 mg per batch (FOS_{small} in 5 mL), 225 mg per batch (FOS_{medium} in 15 mL), and 3 g per batch (FOS_{large} in 0.2 L) (Figure 5A). All of these particle

https://doi.org/10.1021/acsnano.2c10388
ACS Nano XXXX, XXX, XXX−XXX

A

FOS manufactured at different batch sizes

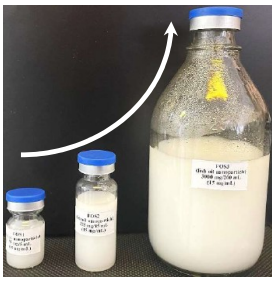

Batch Size: 5 mL (small) 15 mL (medium) 200 mL (large)

Sample	Volume (mL)	Hydrodynamic size (nm)	PDI	Z-potential (mV)	Application
FOS_{small}	5	87.0 ± 1.2	0.21 ± 0.01	-39.0 ± 1.2	Cellular study Mouse study
FOS_{medium}	15	90.2 ± 1.1	0.20 ± 0.01	-26.5 ± 0.9	Cellular study Robust rodent study
FOS_{large}	200	105.7 ± 2.5	0.21 ± 0.01	-24.5 ± 0.6	IND-enabling big animal tox

B

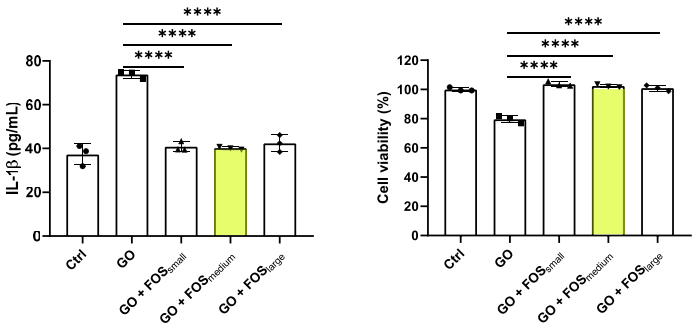

C

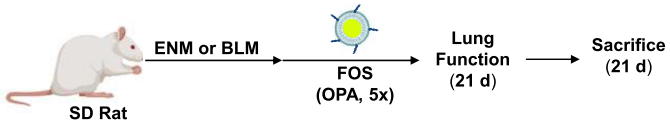

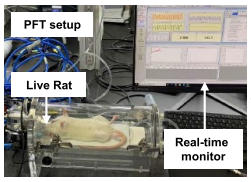

Categories	Parameters
Expiratory phase	FVC, PEF, FEV0.1/FVC R_L, Cchord
Inspiratory phase	IC
General indicators	TV

D

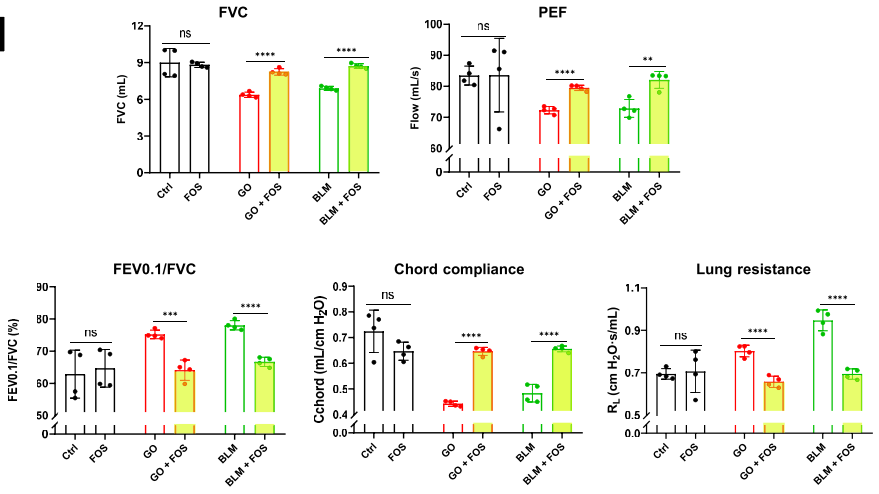

Figure 5. continued

https://doi.org/10.1021/acsnano.2c10388
ACS Nano XXXX, XXX, XXX−XXX

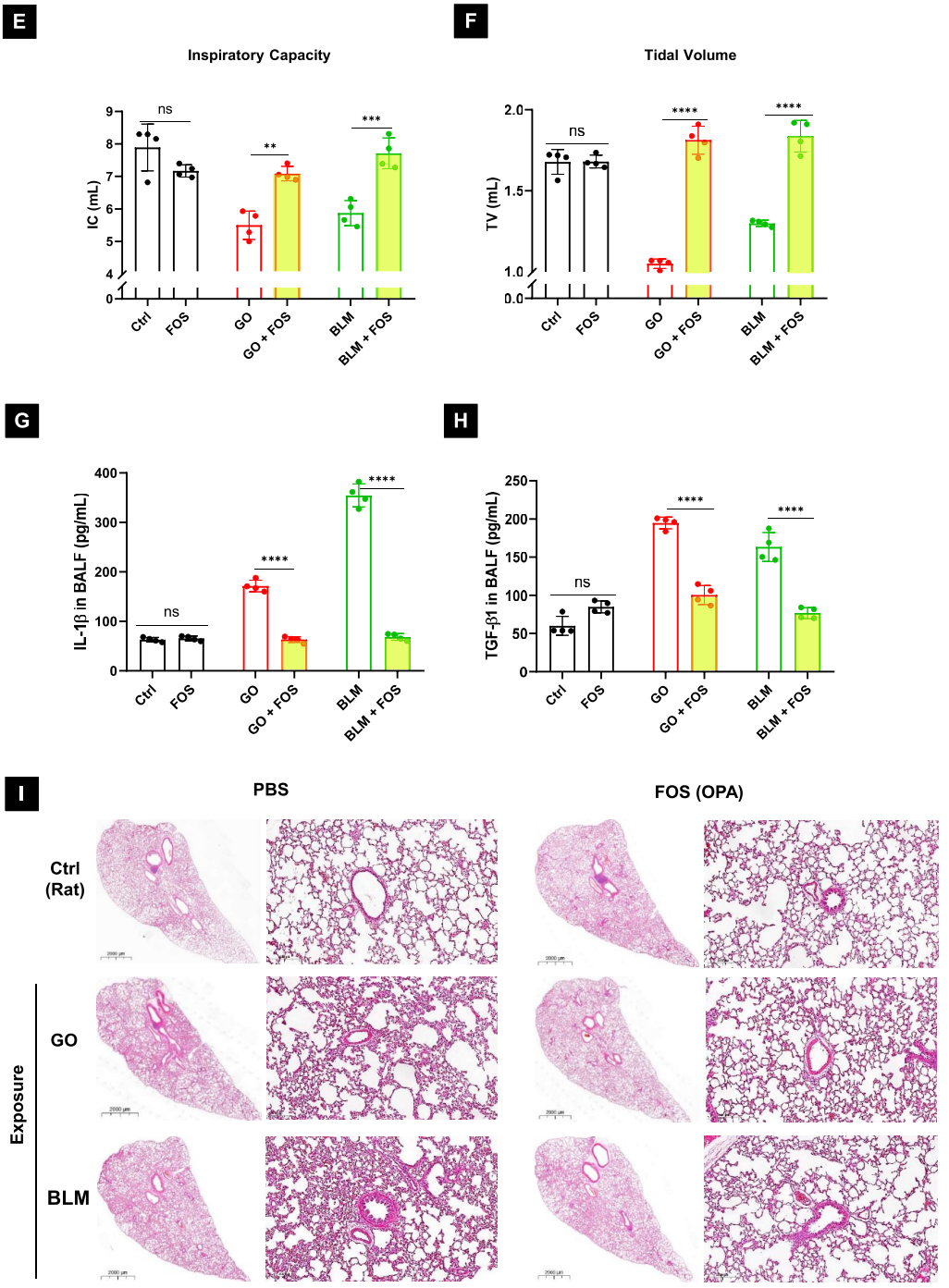

Figure 5. Major improvement of pulmonary function and PF status in a fibrogenic rat model during treatment with FOS. (A) Synthesis of FOS at different quantities. This included the manufacture at 75 mg per batch (FOS_{small} in 5 mL), 225 mg per batch (FOS_{medium} in 15 mL), and 3 g per batch (FOS_{large} in 0.2 L). The physicochemical properties and application of these FOSs are summarized in the inserted table. (B) Before the animal test, all three FOS samples were checked for IL-1β reduction and cell viability restoration in lung macrophages. (C) Experimental setup of fibrogenic rats receiving FOS treatment followed by live animal pulmonary function testing (PFT) and postsacrifice evaluation. In the rat study, six-week-old SD rats (~200 g) received 3 mg/kg GO or bleomycin as PF inducers. Detailed animal study procedures were outlined in the Methods section. The PFT (eSpira Forced Maneuvers system) was carried out on day 21 to real-time monitor the changes in the expiratory phase, inspiratory phase, and general indicators among different groups. After that, rats were sacrificed to collect BAL fluid, serum, and lung tissues. (D–F) PFT data in rats. FOS significantly improved rat lung function in GO- or BLM-induced PF. This was evidenced by the expiratory phase parameters, such as FVC, PEF, FEV0.1/FVC, Chord compliance, and lung resistance (D), the inspiratory phase parameters such as inspiratory capacity (E), and general indicators including TV (F). Additional parameters appear online (Figure S17). (G–I) Assessment of IL-1β (G), TGF-β1 (H), and lung histology (I) from rats receiving indicated treatments. Graphs show the mean ± SEM. Data are analyzed using a two-tailed Student's *t* test. *$p < 0.05$, **$p < 0.01$, ***$p < 0.001$, ****$p < 0.0001$, and "ns" indicates no significance.

batches exerted similar physicochemical properties. Due to the highly potent anti-PF activity that could be achieved at ng/mL concentration, FOS_{medium} allowed us to conduct robust animal work, while FOS_{large} could be used for scale-up research such as a

https://doi.org/10.1021/acsnano.2c10388
ACS Nano XXXX, XXX, XXX−XXX

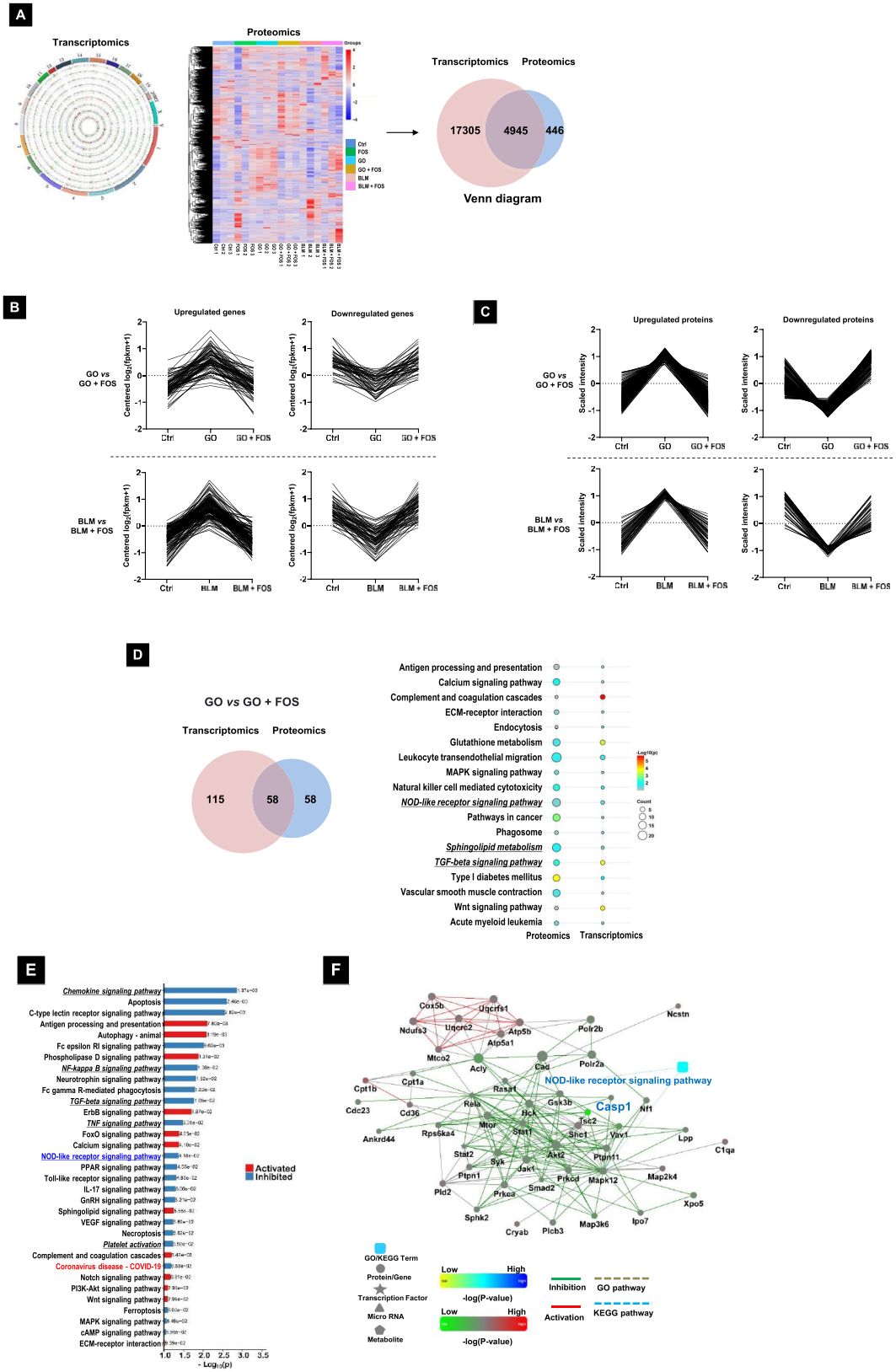

Figure 6. Use of multiomics approaches to reveal the working mechanism of FOS in rat lungs. (A) The Circos, heatmap, and Venn diagram to compare the 22,250 genes identified in transcriptomics and 5391 proteins identified in proteomics, respectively. The Circos data display, the red and green histogram, and gray scatter indicate the upregulated, downregulated, and nonsignificant genes, respectively. In the heatmap, the red, white, and blue colors represent the upregulated, nonsignificant, and downregulated proteins, respectively. (B) In the DEG data display, a general trend is that GO- or BLM-induced upregulated (left) or downregulated (right) genes were restored to the control levels after FOS treatment. The relative intensity values of genes were Z score normalized. (C) Similar to (B), upregulated (left) or downregulated (right) proteins were restored with FOS treatment. (D) Combined analysis of DEGs and DEPs after FOS treatment in GO-exposed rats. This is

https://doi.org/10.1021/acsnano.2c10388
ACS Nano XXXX, XXX, XXX−XXX

Figure 6. continued

demonstrated by the Venn gram to compare KEGG pathways identified in transcriptomics and proteomics (left) and the bubble diagram for representative common pathways (right). (E) Major SPIA to demonstrate the overall activation or inhibition possibility of the signaling pathway regulated by FOS treatment. The italics and underlines demonstrate the pathways that were experimentally tested in Figures 4B−D and 5E−G. The blue underlines indicate the additionally found pathways that would be involved during FOS treatment. We also discovered the FOS's role in COVID-19-related pathways (highlighted in red). (F) Representative functional protein−protein network analysis of DEPs in the NOD-like receptor signaling pathway identified in SPIA. The green and red lines indicate the inhibition and activation functions, respectively.

large animal toxicity study. Before utilization *in vivo*, we also assessed IL-1β reduction and cell viability restoration in lung macrophages that were challenged by GO. All three samples were equally potent *in vitro* (Figure 5B).

As an immediate next step of the mouse study, we selected a 15 mL batch (FOS_{medium}) to conduct the rat work. Meanwhile, we used GO as well as BLM to induce PF in rats, followed by FOS treatment (Figure 5C). In addition to conventional histological and biochemical studies in mice, the higher animal body weight of rats also allowed the performance of pulmonary function testing, a clinically relevant assessment of the respiratory system in live animals and PF patients.[33−35] The results demonstrated that the larger-batch FOS treatment significantly blocked various adverse effects concerning the expiratory phase, inspiratory phase, and general indicators in GO- or BLM-treated rats; some of the function parameters returned to the healthy level. Specifically, this includes the forced vital capacity (FVC), peak forced expiratory flow (PEF), forced expiratory volume (FEV) in 0.1 s/FVC, lung resistance, Chord compliance, inspiratory capacity, and tidal volume (Figure 5D−F and Figure S22). Biochemically, we repeated the essential assays to evaluate the effect of FOS in rats. Both IL-1β (Figure 5G) and TGF-β1 (Figure 5H) production were significantly reduced after FOS treatment in BALF and serum (Figure S23). The anti-PF effects of FOS were further confirmed by histology images (Figure 5I). Noteworthy, empty FOS controls did not generate any abnormality or gross pathology, indicative of biocompatibility *in vivo*. Taken together, the bigger batch of FOS generated satisfactory *in vivo* anti-PF efficacy and safety data in rats, in line with the mouse data generated using a smaller FOS batch.

Multiomics Analyses Combined with Biochemical Assays Confirm the Anti-PF Mechanisms. To comprehensively elucidate the anti-PF mechanism of FOS, we conducted RNA sequencing (RNA-Seq)-based transcriptomics and data-independent acquisition (DIA) mass spectrometry-based quantitative proteomics experiments using the rat lung samples shown in Figure 5. The combined use of different omics methods could thoroughly provide mechanistic insight to fully understand an emerging therapy, particularly nanotherapy.[36] This effort has allowed us to identify 4945 common targets between transcriptomics and proteomics data (Figure 6A). Based on the magnitude of the differentially expressed genes (DEGs) analysis, overall, the OPA of FOS recuperated the levels of GO- or BLM-induced gene expression, similar to the control (Figure 6B). The most prominent changed genes are outlined in Figure S24, including the identified platelet-activating factor receptor activity-related gene (*pdgfrl*) and collagen trimer-related gene (*col5a3*), which were in agreement with the biochemicals discovered in rat studies. As expected, among DEGs listed in Table 1, we also identified *Cmklr1* (RvE receptor), *S1pr1* (S1P receptor), and others, which were significantly influenced by FOS treatment (Figure S25). Correspondingly, the proteomics data also generated a sharp

Table 1. Summary of Differential Expression Genes (DEGs) under Various Treatments[a]

group	upregulated	downregulated	total	no difference
Ctrl vs GO	48	51	99	17,757
GO vs GO + FOS	32	27	59	17,651
Ctrl vs BLM	53	58	111	17,756
BLM vs BLM + FOS	86	133	219	17,647

[a]DEGs indicate genes $|\log_2$ fold change$| \geq 1$ and $p < 0.05$.

difference in the fibrogenic rat lungs with and without the OPA of FOS (Figure 6C). This allowed us to confirm the changes of anti-inflammatory and antifibrogenic effects, evidenced by Cmklr1, Caspase-1, Smad2, and collagen among others (Figure S26), which correlates to the murine data in the efficacy experiment (Figures 1A−C, 2D, and 4D). Interestingly, many differential expression proteins (DEPs) listed in Table 2 were

Table 2. Summary of Differential Expression Proteins (DEPs)[a]

group	upregulated	downregulated	total	no difference
Ctrl vs GO	370	112	482	4830
GO vs GO + FOS	364	529	893	4419
Ctrl vs BLM	179	211	390	4922
BLM vs BLM + FOS	107	69	176	5136

[a]DEPs indicate proteins with fold change > 1.5 or fold change < 1/1.5, and $p < 0.05$.

subcellular and localized on the membrane or in the cytoplasm, suggesting the major effects of FOS on the membranal or cytoplasmic proteins (Figure S27). The gene ontology enrichment further showed that these DEGs and DEPs are involved in the arachidonic acid metabolism, G protein-coupled receptor (GPCR) binding, TNF-mediated signaling pathway, cytokine production, sphingolipid biosynthetic process, response to TGF-β, collagen-containing extracellular matrix, etc. (Figures S28 and S29). Also, the combined Kyoto Encyclopedia of Genes and Genomes (KEGG) analysis of DEGs and DEPs confirmed the inflammation- and fibrosis-related pathways affected by FOS in GO- (Figure 6D) and BLM-exposed (Figure S30) rats. Furthermore, the signaling pathway impact analysis (SPIA) data demonstrated that FOS treatment inhibited the NOD-like receptor, NF-κB, TNF, TGF-β signaling pathway, etc. (Figure 6E), supported by their functional protein−protein network analysis in Figure 6F and Figure S31. As expected, the Reactome results also indicated that FOS treatment enhanced the SPM biosynthesis, collagen degradation, etc., promoting anti-PF effects (Figure S32).

Consistent with the biochemical assays, we have discussed the confirmatory hits during omics data interpretation, such as NLRP3 inflammasome activation, the NF-κB pathway, and TGF-β signaling. Equally important, other mechanisms also

https://doi.org/10.1021/acsnano.2c10388
ACS Nano XXXX, XXX, XXX−XXX

emerged in the omics data, demonstrating how FOS perturbs multiple pathways and results in a broad activation of anti-PF processes. This includes pathways that were not explored before. To name a few, while detoxification of ROS showed up in Figures S28, S29, and S32, we discerned a recovery pattern on phospholipase C (PLC) activation and calcium ion binding in Figures S28 and S29. We also observed a prominent effect on ceramide biosynthesis according to Figure S29 (highlighted in blue). These omics-identified additional hits inspired us to look at the inhibitory effects of RvD1, RvE1, and FOS on the lipid peroxidation in animal lungs and macrophages (Figure S33), the PLC activity and calcium ion influx (Figure S34), and mitochondrial ROS (mtROS) production in alveolar macrophages (Figure S35). Similarly, biochemical assays in Figure S36 demonstrated the beneficial effects of free resolvins and FOS on blocking ENMs-induced ROS or ceramide (a main molecule in the TGF-β pathway) in epithelial cells.

DISCUSSION

In this study, we developed a biocompatible SPMs-based pulmonary drug nanocarrier for PF treatment and validated its efficacy and safety at the cellular and intact animal levels. This was evidenced by the comprehensive investigation from a biochemical, histological, multiomics, and more importantly functional standpoint. This work is innovative because it represents a rising and substantive departure from the prior stae-of-the-art, namely, the use of a nano-enabled approach to implementing resolvin biology to develop a translationally useful inhalable nanomedicine candidate to alleviate PF, induced by occupational inducers and chemical drugs. With respect to the working mechanism of FOS, the biochemistry assays and omics data indicated that the lipid peroxidation-triggered NLRP3 inflammasome activation interacting with the NF-κB pathway was the targeted process for resolvins and FOS during the anti-PF *in vitro* and *in vivo* (Figure S37). We proposed that this involved the PLC activation, calcium flux, mtROS generation, caspase-1 activation, IL-1β release as well as the TNF-R1 expression, NF-κB activation, and TNF-α secretion in macrophages.[10,37] Moreover, resolvins and FOS also interfered with the ROS-mediated TGF-β/Smad and S1P signaling pathways in epithelial cells, involving the production of ROS, ceramide, S1P, TGF-β, and p-Smad2/3 (Figure S38).[38−40]

From the biocompatibility perspective, our carrier design is advantageous because we deliberately selected a biocompatible lipid-based formulation based on the combination of FDA readiness of fish oil and the alveoli microenvironment, which abundantly contains lipids among other biomolecules. For example, omega-3-containing fish oil has been FDA-approved for the oral dosage form of Lovaza and intravenously injectable form of Omegaven.[29−32] To increase drug permeability through the lung epithelium, the final formulation also includes phosphatidylcholine (lecithin), the building block of dipalmitoylphosphatidylcholine, which is the primary lipid component of lung surfactant, and polyethyleneglycol (PEG) to make it easier for nanoparticles to cross the mucosal barrier.[2−5] Additionally, we have included empty FOS as a control (Figures 3−6) to show the biocompatibility of the empty nanocarrier; FOS did not generate any cytotoxicity, abnormality, or gross pathology.

While nanoformulation is offering great promise, in certain areas becoming a paradigm shift for disease management, chemistry, manufacturing, and controls of nanotherapeutics (nano-CMC) become critical "checkpoints" for translational nanomedicine. Planning a successful nano-CMC requires a long list of considerations, which in this case include raw material selection, scale-up synthesis routes, batch size, stability control, release criteria, analytical method, documentation, etc. We have streamlined the FOS production to a status that allows robust animal work, as well as an Investigational New Drug Application (IND)-enabling study that is planned at this moment. Based on the rodent data and dosage conversion index,[41] we were able to translate the quantities that will be required for the investigation of big animals (e.g., ferrets or monkeys) and human beings (Figure S39). For example, we expect that our 0.2 L batch would be enough to treat ∼70 monkeys or ∼700 ferrets with PF, according to the mouse/rat data. We foresee a further scale-up to achieve an even larger batch, if necessary. The easiest way is to set up parallel equipment or upgrade our procedures using automated flow-through sonication and/or microfluidic systems.[42]

Based on the working mechanism of nanosized SPM, we envisage how nano-enabled SPM therapy can be leveraged in other disease scenarios. To name a few, omics data have identified a comprehensive list of targeted pathways (Figure 6), which includes the COVID-19 pathway (Figure 6E, highlighted in red), implying the potential role of FOS in treating SARS-CoV-2-induced inflammation and PF.[21,23] Moreover, a particulate form of resolvin therapy could be useful in treating different diseases that involve inflammation, such as liver fibrosis, inflammatory bowel disease, arthritis, thrombosis, and even cancer, considering the inflammation resolution of resolvins and FOS in various macrophages such as Kupffer, RAW264.7, J774.A1, and THP-1 cells. In this regard, versatile SPM nanodesign approaches could be theoretically possible, such as encapsulation of SPM derivatives, precursors, prodrugs, SPM/drug combinations, etc. Taken together, using nanotoxicity discovery to design an inhalable nanomedicine candidate which is validated in cell culture and mice and rats, this dynamic but logically connected design makes this study have a broad interest in treating life-threatening diseases.

STUDY LIMITATIONS

Before we conclude, we briefly comment on the limitations of this investigation. There are pros and cons of using fish oil to formulate inhalable nanoparticles. Fish oil is easy to obtain, has FDA-approved applications (for IV or oral dosage form), is easy to formulate, and is therapeutically potent; however, the composition is complex.[30−32] For example, fish oil could convert into other SPMs with ∼47 identified single members, which demands further research.[43,44] While similar studies about the effects of resolvins and nano-fish oil were recently reported,[20,22,27,31] the nano-enabled approach to implementing resolvins' biology to develop a translationally useful inhalable nanomedicine candidate based on the leveraged use of nanotoxicology discovery with clear mechanisms has not been explored before. From a (nano)drug development perspective, we are still in the proof-of-concept stage intending to identify a lead "nanoformulation". It is necessary to further update the formulation by optimizing the formulation factors such as the resolvin source, ratio, lipid composition, charge, and size by considering potency, safety, IND application pathway, etc., which could not be conveniently achieved without the current work. This is likely to be achieved via a high-throughput screening process, allowing the identification of ready-to-translate products for chemistry, manufacturing, and controls (CMC), the official GMP manufacturer, and a clinical trial.

https://doi.org/10.1021/acsnano.2c10388
ACS Nano XXXX, XXX, XXX−XXX

Further research would also include how the prepared nanoparticles interact with lung surfactants, considering any oily aerosols that are directly delivered into the lungs might fluidize the pulmonary surfactant film of the lung.[43] It would be interesting to investigate the role of the "biological corona", which in the case of the lungs could involve lipids, proteins, and nuclear acids. In addition to mice and rats, we will use a scale-up, quality-controlled final product to confirm our data in advanced animal models, such as ferrets.[28,41,42] Also, considering the long-lasting and progressive properties of ENMs-induced PF, the long-term effect of a resolvin-derived nanomedicine should be conducted in the future.

CONCLUSIONS

In summary, we demonstrated the establishment of an inhalable and scalable pulmonary delivery FOS nanoparticle that targets SPM pathways, which are highly efficacious in ENM- and BLM-induced PF in mice and rats. This is achieved by the synthesis of lipid-based and biocompatible nanoparticles containing an FDA-approved resolvin precursor, fish oil, based on the combined considerations of alveoli microenvironment, formulation practicability, stability, cost, scalability, reproducibility, effectiveness, and safety. Furthermore, the OPA and inhalation of FOS nanoparticles demonstrated sufficient biodistribution in the lungs; this resulted in markedly improved anti-inflammatory status, histological characteristics, and importantly pulmonary function, with satisfactory nanosafety profiles *in vitro* and *in vivo*. Mechanistic studies by multiomics analyses and biochemical assays insightfully indicated that the protective effects of FOS, similar to resolvins, were attributed to their interference with the lipid peroxidation-trigged NLRP3 inflammasome activation and NF-κB pathways along with the ROS-mediated TGF-β/Smad and S1P signaling pathways. This work has excellent potential for translation in the clinic.

METHODS

Cell Culture. The alveolar macrophages were cultured in high-glucose Dulbecco's modified Eagle medium (DMEM) with supplemented with 10% fetal bovine serum (FBS; Gemini Bio-Products) and 100 U/mL to 100 μg/mL penicillin−streptomycin (P/S) at 37 °C in a humidified 5% CO_2 atmosphere. The human lung epithelial cell line, BEAS-2B, was obtained from ATCC and cultured in bronchial epithelial basal medium (BEBM) (Lonza, IL, USA) supplemented with growth factors from the Single Quots kit (Lonza). RvD1 (No. 10012554) and RvE1 (No. 10007848) purchased from the Cayman Chemical Company, as well as fish oil (No. F8020) purchased from Sigma, were used to pretreat cells for *in vitro* studies.

Determination of IL-1β Secretion, Caspase-1 Activation, and TNF-α Release in Macrophages. Various macrophages, including alveolar macrophages seeded at a density of 3×10^4 cells/well in a 96-well plate, were primed by 1 μg/mL lipopolysaccharide (LPS) for 4 h to initiate transcription of the pro-IL-1β (IL-1β precursor) and exposed to a 12.5 μg/mL GO or Gd_2O_3 nanoparticle suspension containing 0.1 μg/mL LPS for 24 h. Cellular supernatants were collected for IL-1β and TNF-α quantification by ELISA, respectively, according to the manufacturer's instructions of the mouse IL-1β/IL-1F2 DuoSet ELISA kit (DY401) and the mouse TNF-α DuoSet ELISA (DY410) from R&D Systems Inc. Concentrations in these determinations were expressed as picograms per milliliter (pg/mL). For the evaluation of caspase-1 activity, treated cells with resolvins and ENMs were incubated with FAM-FLICA caspase-1 substrates (ImmunoChemistry Technologies) for 1 h at 37 °C. The quantified fluorescence intensity in cells was monitored at an excitation/emission wavelength of 492/520 nm.

Assessment of TGF-β1, S1P, and Smad2/3 Phosphorylation Levels in Epithelial Cells. For the assessment of S1P and TGF-β1 levels in epithelial cells, BEAS-2B cells treated with/without 100 ng/mL resolvins for 0.5 h were incubated with 12.5 μg/mL ENMs for 24 h. The supernatants were collected to determine S1P and TGF-β1 production using ELISA assays, as previously reported.[24,25,40] Concentrations in these determinations were expressed as pg/mL. For Smad2/3 phosphorylation, cells treated with resolvins and ENMs were collected and lysed. The evaluation of Smad2/3 phosphorylation was performed by an ELISA kit (No. 12001C) from Cell Signaling Technologies Inc.[46]

siRNA Knockdown and Pharmacological Inhibition Experiments to Determine the Role of Resolvin Receptors. Various resolvin receptors in macrophages were knocked down using siRNA according to the literature.[37] We focused on the RvD1 receptor (ALX4) and the RvE1 receptor (CMKLR1), which are the main specialized GPCRs for RvD1 and RvE1 in mice macrophages, respectively. Briefly, 10 μL of 200 ng/mL of each of the siRNA in buffer purchased from Sigma was delivered into 1×10^6 cells via electroporation. After electroporation, cells were maintained in a complete medium for another 48 h before further use. To rule out the unwanted effects during the knockdown experiment, a siRNA that was designed to target a rat gene (LTB4R) was included as an additional control. Knockdown efficiency and cell viability (MTS assay) during the siRNA experiment were assessed to safeguard our data quality. Moreover, to show the role of the RvD1 receptor in epithelial cells, BOC-2 (MP Biomedicals), the RvD1 receptor antagonist, was used at 10 μM to treat BEAS-2B cells for 30 min before the RvD1 incubation.

Demonstration of Anti-PF Effect Using Resolvins in Mice. Eight-week-old male C57BL/6 mice were housed under standard laboratory conditions (23 ± 2 °C; 60% relative humidity; 12 h/12 h light/dark cycle) and hygiene status (autoclaved food and acidified water). The mouse exposure to GO or Gd_2O_3 nanoparticles was carried out by the oropharyngeal aspiration method.[24,25,28] Briefly, animals were anesthetized by an intraperitoneal injection of ketamine (100 mg/kg). With the anesthetized animals held in a vertical position, 40 μg of nanoparticle suspension (50 μL) was instilled at the back of the tongue to allow access to the oropharynx and prevent swallowing of the inoculum to the side for pulmonary aspiration. Twenty-four hours post-ENM exposure, resolvins were daily administered by OPA at a dose of 5 μg/kg from day 1 to day 5.

The animal experiment was concluded on day 21 for BALF and lung tissue collection as previously described.[45] Briefly, the trachea was cannulated, and the lungs were gently lavaged three times with 1 mL of sterile PBS to obtain the BALF. The supernatant and cell pellets of the first lavage were collected after centrifugation. The collected supernatant was then used for the determination of IL-1β, MCP-1 (DY479, R&D Systems), MMP-9 (MMPT90, R&D Systems), TGF-β1 (DY1679, R&D Systems), and PDGF-AA (LS-F38385, LSBio Inc.) levels according to the manufacturer's protocols, respectively. Lung tissues were collected, embedded, sectioned, and stained with H&E for lung morphology or with MT to determine the collagen deposition.[24,25] The obtained lung tissues were also used for the assessment of α-SMA by the mouse α-smooth muscle actin ELISA kit (NBP266429, Novus Biologicals LLC), and total collagen content was determined by the Sircol soluble collagen assay kit (Biocolor Ltd., UK).[24] The hydroxyproline level in lung tissue samples was measured using a colorimetric hydroxyproline assay kit (ab222941, Abcam). All samples were assayed in duplicate, and results were expressed as the mean of nanograms per milligram of protein.

Determination of Specialized Pro-Resolving Lipid Mediators. The levels of RvD1 and LXA4 in macrophage cell culture supernatant or BALF were quantified by ELISA kits from Cayman Chemical Company (No. 500380 for RvD1 and No. 590410 for LXA4). The concentrations of RvD1 or LXA4 in the samples were calculated by their absorbance at a wavelength of 414 nm as well as the corresponding standard curves.[47,48]

Preparation and Characterization of Fish Oil Nanoparticles at Different Quantities. FOS nanoparticles were prepared by a single emulsification/solvent evaporation method.[32,49] Briefly, 75 mg of fish oil, 25 mg of lecithin (No. 429415, Sigma), and 1.25 mg of DSPE-PEG (No. 880120C, Avanti Polar Lipids) were dissolved in 2.5 mL of chloroform. Subsequently, this solution was hydrated by addition to the

https://doi.org/10.1021/acsnano.2c10388
ACS Nano XXXX, XXX, XXX−XXX

aqueous phase containing 5 mL of deionized water and 5 mg of Tween 80, followed by water bath sonication for 15 min. The mixture was maintained and homogenized under magnetic stirring for 1 h; this will allow sufficient solvent diffusion and the formation of an O/W emulsion. The resultant dispersions were emulsified by a probe sonicator that delivers a power output of 60 W and a 5/15 s on/off working pulse on ice for ∼45 min. Organic solvents were eliminated by evaporation under reduced pressure with a rotary evaporator at 45 °C for ∼1 h. The obtained hydrophilic suspension was further sonicated in a water bath sonicator. The final FOS nanoparticle suspension was kept at 4 °C for future use. To visualize the distribution of FOS, we also prepared fluorescently labeled FOS by adding 2% (w/w) Cy5.5 PE (No. 810346, Avanti Polar Lipids) to the lipid.

To make FOS_{medium} and FOS_{large}, we proportionally increased the raw material feed ratio and tinkered with the protocol, with minor modifications. For making FOS_{medium}, 225 mg of fish oil, 75 mg of lecithin, and 3.75 mg of DSPE-PEG were dissolved in 7.5 mL of chloroform and hydrated by a mixture of 15 mL of deionized water and 15 mg of Tween 80. The raw materials for making FOS_{large} included 3000 mg of fish oil, 1000 mg of lecithin, 50 mg of DSPE-PEG, 100 mL of chloroform, 200 mL of deionized water, and 200 mg of Tween 80. To ensure the colloidal stability and dispersion of FOS_{medium} and FOS_{large} samples, we used an 80 W probe sonication for 60 and 90 min, respectively. FOS nanoparticles were fully characterized before biological experiments. The morphology, size, PDI, zeta potential, and stability were characterized by cryogenic electron microscopy (cryo-EM) and dynamic light scattering (DLS), respectively. We also looked at the size and PDI upon storage at 4 °C. Moreover, the encapsulation efficiency (EE) was calculated by the following equation: $EE\ (\%) = W_{\text{encapsulated fish oil}}/W_{\text{total fish oil}} \times 100\%$, where $W_{\text{encapsulated fish oil}}$ represents the weight of fish oil encapsulated in the nanoparticles and determined by the Stewart assay, while $W_{\text{total fish oil}}$ represents the fish oil added initially in the particle formation mixture.[32,50]

Assessment of FOS Effects *in Vivo* and *in Vitro*. FOS nanoparticles were used to investigate their efficacy and safety. Before animal experimentation, we first looked at the cellular responses of FOS nanoparticles in lung macrophages and epithelial cells receiving different ENMs. In the case of FOS at different batch sizes, a similar check was performed with respect to cell viability evaluation and the IL-1β ELISA assay. This was followed by the biodistribution study in healthy mice, which were OPA administrated with a Cy5.5-labeled FOS at 2.5 mg/kg. Both intact animal imaging and *ex vivo* imaging were performed at 4 and 24 h using an IVIS imager. In the efficacy study, the effects of FOS on inflammation resolution and fibrogenesis improvement were determined by the same methods used for the resolvins described above. GO-treated fibrogenic mice received 50 μL of FOS (1 mg/mL) through the OPA for 5 consecutive days. In this case, although we only determined the FOS effect in the GO-induced PF model, we compared the therapeutic benefits of OPA vs IP by adding identical doses and treatment frequency.

Pulmonary Function and Efficacy Assessment of FOS Effects in Rats. Six-week-old female pathogen-free Sprague−Dawley (SD) rats were obtained and housed in a standard animal facility. Following an approximately 1 week acclimatization period, rats were exposed to 3 mg/kg GO or bleomycin (Sigma) using the OPA method described above. The treatment dose was ∼2.5 mg/kg, and the frequency was the same as that of the mouse.

The eSpira forced maneuvers system (EMMS, Borden, UK) was used to evaluate the PFT in live rats. Briefly, an IP injection of pentobarbital sodium (50 mg/kg) was used to anesthetize rats. The tracheas were then cannulated, and each rat was attached to a small-animal ventilator operated by a computer. Also, rats were permitted to breathe on their own and were monitored with a pneumotachograph coupled to a transducer in a whole-body plethysmograph. Then, an esophageal catheter was used to measure the transpulmonary pressure. The eDaq software (EMMS) was used to compute baseline airway resistance, and baseline lung function was assessed for 1 min. The real-time monitoring of multiple parameters relating to the expiratory phase, inspiratory phase, and general indicators was carried out during the PFT. After the PFT study, IL-1β and TGF-β1 in BALF and serum were quantified by the rat IL-1β ELISA kit (No. ERC007.96, Neobioscience Technology) and the QuantiCyto rat TGF-β1 ELISA kit (No. ERC107b.96, Neobioscience Technology).

RNA Sequencing-Based Transcriptomics and DIA Mass Spectrometry-Based Proteomics Analyses of Rat Lungs. To fully elucidate the working mechanism of FOS nanoparticles, we used a combined approach to look at transcriptional and protein expression patterns in rat lungs after different treatments. For the transcriptomic analysis, total RNA was extracted from each rat lung sample in the control, FOS, GO, GO + FOS, BLM, and BLM + FOS groups, using Trizol reagent (Invitrogen) or an RNeasy mini kit (Qiagen). Then RNA sequencing and analysis were performed by Shanghai Bioprofile Technology Co., Ltd. The genes with a p-value less than 0.05 and a |log 2 fold change| larger than 1 were identified as DEGs in this study. Gene ontology enrichment and KEGG pathway analysis of DEGs were annotated according to the hypergeometric distribution.

In the proteomics study, the same aliquots from the 18 rat tissue samples were used for protein extraction. These protein samples were subjected to digestion, desalination, and peptide separation and recognition by LC-MS, followed by proteomic analysis from the company. Briefly, the obtained MS data were analyzed using MaxQuant software version 1.6.0.16 and searched against Uniprot-*Rattus norvegicus* (rat) [10116]-36254-202204.FASTA. For database searches, the maximum of two missed cleavage sites was set at 4.5 ppm for precursor ions and 20 ppm for fragment ions. At the peptide-spectrum-matched and protein levels, the database search results were filtered and exported with less than a 1% false discovery rate. MaxQuant was used to do label-free quantification utilizing an intensity determination and normalizing technique. The quantitative protein ratios were weighted and normalized using the median ratio in Maxquant software. Only proteins having a fold change of more than 1.5 and a p-value of less than 0.05 were considered to have significantly different expressions. To annotate the sequences, information was extracted from UniProtKB/Swiss-Prot, and gene ontology, KEGG, SPIA, and Reactome analyses were carried out with Fisher's exact test. The construction of protein−protein interaction networks was also conducted by using the STRING database with Cytoscape software. This forms the bases of data displayed in Figure 6. The detailed methodology appears in the supporting methods.

Statistical Analysis. GraphPad Prism version 8.0.1 was used to analyze all of the data. A two-tailed Student's t test for two-group analysis or a one-way ANOVA for multiple-group comparisons was used to establish statistical significance, which is defined as a p-value of less than 0.05.

ASSOCIATED CONTENT

Supporting Information

The Supporting Information is available free of charge at https://pubs.acs.org/doi/10.1021/acsnano.2c10388.

Supplementary figures, supporting information and methods, and supplementary references (PDF)

AUTHOR INFORMATION

Corresponding Authors

Tian Xia − *Division of NanoMedicine, Department of Medicine, University of California, Los Angeles, California 90095, United States*; orcid.org/0000-0003-0123-1305; Email: txia@ula.edu

Huan Meng − *CAS Key Laboratory for Biomedical Effects of Nanomaterials and Nanosafety, CAS Center for Excellence in Nanoscience, National Center for Nanoscience and Technology, Beijing 100190, People's Republic of China*; orcid.org/0000-0001-8844-3938; Email: mengh@nanoctr.cn

https://doi.org/10.1021/acsnano.2c10388
ACS Nano XXXX, XXX, XXX−XXX

Authors

Jiulong Li − *CAS Key Laboratory for Biomedical Effects of Nanomaterials and Nanosafety, CAS Center for Excellence in Nanoscience, National Center for Nanoscience and Technology, Beijing 100190, People's Republic of China;* orcid.org/0000-0002-8816-7539

Yu Xiao − *CAS Key Laboratory for Biomedical Effects of Nanomaterials and Nanosafety, CAS Center for Excellence in Nanoscience, National Center for Nanoscience and Technology, Beijing 100190, People's Republic of China; University of Chinese Academy of Sciences, Beijing 100049, People's Republic of China*

Yumo Zhang − *CAS Key Laboratory for Biomedical Effects of Nanomaterials and Nanosafety, CAS Center for Excellence in Nanoscience, National Center for Nanoscience and Technology, Beijing 100190, People's Republic of China; Department of Environment and Life, Beijing University of Technology, Beijing 100124, People's Republic of China*

Silu Li − *CAS Key Laboratory for Biomedical Effects of Nanomaterials and Nanosafety, CAS Center for Excellence in Nanoscience, National Center for Nanoscience and Technology, Beijing 100190, People's Republic of China; Department of Pharmacy, The First Affiliated Hospital of Zhengzhou University, Zhengzhou 450052 Henan, People's Republic of China*

Minzhi Zhao − *CAS Key Laboratory for Biomedical Effects of Nanomaterials and Nanosafety, CAS Center for Excellence in Nanoscience, National Center for Nanoscience and Technology, Beijing 100190, People's Republic of China*

Complete contact information is available at: https://pubs.acs.org/10.1021/acsnano.2c10388

Author Contributions

Conceptualization: JL, TX, HM; methodology: JL, TX, HM; investigation: JL, YX, YZ, SL; funding acquisition: JL, TX, HM; project administration: JL, TX, HM; supervision: TX, HM; writing−original draft: JL; writing−review and editing: JL, MZ, TX, HM.

Notes

The authors declare no competing financial interest.

ACKNOWLEDGMENTS

The authors acknowledge financial support from the National Key Research and Development Program of China (2022YFA-1207300, 2021YFA1200902). We want to thank the support from the National Natural Science Foundation of China (32271449 and 32201172), the start-up funding support from the National Center for Nanoscience and Technology, Chinese Academy of Sciences (CAS) (E1763911), and the CAS Project for Young Scientists in Basic Research (YSBR-036). The authors would like to thank Yan Gong, Yu Wang, Jidan Huang, Haiqiang Wang, the Shanghai Bioprofile Technology Co., Ltd., and many others for their technical assistance.

REFERENCES

(1) Altorki, N. K.; Markowitz, G. J.; Gao, D.; Port, J. L.; Saxena, A.; Stiles, B.; McGraw, T.; Mittal, V. The lung microenvironment: an important regulator of tumour growth and metastasis. *Nat. Rev. Cancer* **2019**, *19*, 9−31.

(2) Kreyling, W. G.; Hirn, S.; Schleh, C. Nanoparticles in the lung. *Nat. Biotechnol.* **2010**, *28*, 1275−1276.

(3) Melms, J. C.; Biermann, J.; Huang, H.; Wang, Y.; Nair, A.; Tagore, S.; Katsyv, I.; Rendeiro, A. F.; Amin, A. D.; Schapiro, D.; Frangieh, C. J.; Luoma, A. M.; Filliol, A.; Fang, Y.; Ravichandran, H.; Clausi, M. G.; Alba, G. A.; Rogava, M.; Chen, S. W.; Ho, P.; Montoro, D. T.; Kornberg, A. E.; Han, A. S.; Bakhoum, M. F.; Anandasabapathy, N.; Suárez-Fariñas, M.; Bakhoum, S. F.; Bram, Y.; Borczuk, A.; Guo, X. V.; Lefkowitch, J. H.; Marboe, C.; Lagana, S. M.; Del Portillo, A.; Tsai, E. J.; Zorn, E.; Markowitz, G. S.; Schwabe, R. F.; Schwartz, R. E.; Elemento, O.; Saqi, A.; Hibshoosh, H.; Que, J.; Izar, B. A molecular single-cell lung atlas of lethal COVID-19. *Nature* **2021**, *595*, 114−119.

(4) Lederer, D. J.; Martinez, F. J. Idiopathic pulmonary fibrosis. *New Engl. J. Med.* **2018**, *378*, 1811−1823.

(5) Martinez, F. J.; Collard, H. R.; Pardo, A.; Raghu, G.; Richeldi, L.; Selman, M.; Swigris, J. J.; Taniguchi, H.; Wells, A. U. Idiopathic pulmonary fibrosis. *Nat. Rev. Dis. Primers* **2017**, *3*, 17074.

(6) Bazdyrev, E.; Rusina, P.; Panova, M.; Novikov, F.; Grishagin, I.; Nebolsin, V. Lung Fibrosis after COVID-19: treatment prospects. *Pharmaceuticals (Basel, Switzerland)* **2021**, *14*, 807.

(7) George, P. M.; Wells, A. U.; Jenkins, R. G. Pulmonary fibrosis and COVID-19: the potential role for antifibrotic therapy. *Lancet Respir. Med.* **2020**, *8*, 807−815.

(8) Guo, C.; Zhang, C.; Xia, Z.; Song, B.; Hu, W.; Cui, Y.; Xue, Y.; Xia, M.; Xu, D.; Zhang, S.; Fang, J. Nano-designed CO donor ameliorates bleomycin-induced pulmonary fibrosis via macrophage manipulation. *J. Controlled Release* **2022**, *341*, 566−577.

(9) Zhao, H.; Wu, L.; Yan, G.; Chen, Y.; Zhou, M.; Wu, Y.; Li, Y. Inflammation and tumor progression: signaling pathways and targeted intervention. *Signal Transduct. Target.* **2021**, *6*, 263.

(10) Li, J.; Gao, X.; Wang, Y.; Xia, T.; Zhao, Y.; Meng, H. Precision design of engineered nanomaterials to guide immune systems for disease treatment. *Matter* **2022**, *5*, 1162−1191.

(11) Medzhitov, R. Inflammation 2010: New adventures of an old flame. *Cell* **2010**, *140*, 771−776.

(12) Serhan, C. N.; Radin, A.; Smolen, J. E.; Korchak, H.; Samuelsson, B.; Weissmann, G. Leukotriene B4 is a complete secretagogue in human neutrophils: A kinetic analysis. *Biochem. Bioph. Res. Co.* **1982**, *107*, 1006−1012.

(13) Basil, M. C.; Levy, B. D. Specialized pro-resolving mediators: endogenous regulators of infection and inflammation. *Nat. Rev. Immunol.* **2016**, *16*, 51−67.

(14) Chiang, N.; Serhan, C. N. Specialized pro-resolving mediator network: an update on production and actions. *Essays Biochem.* **2020**, *64*, 443−462.

(15) Schwab, J. M.; Chiang, N.; Arita, M.; Serhan, C. N. Resolvin E1 and protectin D1 activate inflammation-resolution programmes. *Nature* **2007**, *447*, 869−874.

(16) Chiang, N.; Fredman, G.; Bäckhed, F.; Oh, S. F.; Vickery, T.; Schmidt, B. A.; Serhan, C. N. Infection regulates pro-resolving mediators that lower antibiotic requirements. *Nature* **2012**, *484*, 524−528.

(17) Panigrahy, D.; Gilligan, M. M.; Serhan, C. N.; Kashfi, K. Resolution of inflammation: An organizing principle in biology and medicine. *Pharmacol. Therapeut.* **2021**, *227*, No. 107879.

(18) Sandhaus, S.; Swick, A. G. Specialized proresolving mediators in infection and lung injury. *Biofactors* **2021**, *47*, 6−18.

(19) Godson, C. Balancing the effect of leukotrienes in Asthma. *New Engl. J. Med.* **2020**, *382*, 1472−1475.

(20) Isopi, E.; Mattoscio, D.; Codagnone, M.; Mari, V. C.; Lamolinara, A.; Patruno, S.; D Aurora, M.; Cianci, E.; Nespoli, A.; Franchi, S.; Gatta, V.; Dubourdeau, M.; Moretti, P.; Di Sabatino, M.; Iezzi, M.; Romano, M.; Recchiuti, A. Resolvin D1 reduces lung infection and inflammation activating resolution in cystic fibrosis. *Front. Immunol.* **2020**, *11*, 581.

(21) Balta, M. G.; Papathanasiou, E.; Christopoulos, P. F. Specialized pro-resolving mediators as potential regulators of inflammatory macrophage responses in COVID-19. *Front. Immunol.* **2021**, *12*, No. 632238.

(22) Galdino De Souza, D.; Santos, D. S.; Simon, K. S.; Morais, J. A. V.; Coelho, L. C.; Pacheco, T. J. A.; Azevedo, R. B.; Bocca, A. L.; Melo-Silva, C. A.; Longo, J. P. F. Fish oil nanoemulsion supplementation attenuates bleomycin-induced pulmonary fibrosis BALB/c mice. *Nanomaterials* **2022**, *12*, 1683.

(23) Koenis, D. S.; Beegun, I.; Jouvene, C. C.; Aguirre, G. A.; Souza, P. R.; Gonzalez-Nunez, M.; Ly, L.; Pistorius, K.; Kocher, H. M.; Ricketts, W.; Thomas, G.; Perretti, M.; Alusi, G.; Pfeffer, P.; Dalli, J. Disrupted resolution mechanisms favor altered phagocyte responses in COVID-19. *Circ. Res.* **2021**, *129*, e54−e71.
(24) Wang, X.; Duch, M. C.; Mansukhani, N.; Ji, Z.; Liao, Y.; Wang, M.; Zhang, H.; Sun, B.; Chang, C. H.; Li, R.; Lin, S.; Meng, H.; Xia, T.; Hersam, M. C.; Nel, A. E. Use of a pro-fibrogenic mechanism-based predictive toxicological approach for tiered testing and decision analysis of carbonaceous nanomaterials. *ACS Nano* **2015**, *9*, 3032−3043.
(25) Li, R.; Ji, Z.; Chang, C. H.; Dunphy, D. R.; Cai, X.; Meng, H.; Zhang, H.; Sun, B.; Wang, X.; Dong, J.; Lin, S.; Wang, M.; Liao, Y.; Brinker, C. J.; Nel, A.; Xia, T. Surface interactions with compartmentalized cellular phosphates explain rare earth oxide nanoparticle hazard and provide opportunities for safer design. *ACS Nano* **2014**, *8*, 1771−1783.
(26) Li, J.; Chen, C.; Xia, T. Understanding nanomaterial−liver interactions to facilitate the development of safer nanoapplications. *Adv. Mater.* **2022**, *34*, No. 2106456.
(27) Yang, Y.; Hu, L.; Xia, H.; Chen, L.; Cui, S.; Wang, Y.; Zhou, T.; Xiong, W.; Song, L.; Li, S.; Pan, S.; Xu, J.; Liu, M.; Xiao, H.; Qin, L.; Shang, Y.; Yao, S. Resolvin D1 attenuates mechanical stretch-induced pulmonary fibrosis via epithelial-mesenchymal transition. *Am. J. Physiol.-Lung C* **2019**, *316*, L1013−L1024.
(28) Shvedova, A. A.; Kisin, E.; Murray, A. R.; Johnson, V. J.; Gorelik, O.; Arepalli, S.; Hubbs, A. F.; Mercer, R. R.; Keohavong, P.; Sussman, N.; Jin, J.; Yin, J.; Stone, S.; Chen, B. T.; Deye, G.; Maynard, A.; Castranova, V.; Baron, P. A.; Kagan, V. E. Inhalation vs. aspiration of single-walled carbon nanotubes in C57BL/6 mice: inflammation, fibrosis, oxidative stress, and mutagenesis. *Am. J. Physiol.-Lung C* **2008**, *295*, L552−L565.
(29) Dalli, J.; Serhan, C. N. Identification and structure elucidation of the pro-resolving mediators provides novel leads for resolution pharmacology. *Br. J. Pharmacol.* **2019**, *176*, 1024−1037.
(30) Bender, N.; Portmann, M.; Heg, Z.; Hofmann, K.; Zwahlen, M.; Egger, M. Fish or n3-PUFA intake and body composition: a systematic review and meta-analysis. *Obes. Rev.* **2014**, *15*, 657−665.
(31) Yan, Y.; Jiang, W.; Spinetti, T.; Tardivel, A.; Castillo, R.; Bourquin, C.; Guarda, G.; Tian, Z.; Tschopp, J.; Zhou, R. Omega-3 fatty acids prevent inflammation and metabolic disorder through inhibition of NLRP3 inflammasome activation. *Immunity* **2013**, *38*, 1154−1163.
(32) Ghorbanzade, T.; Jafari, S. M.; Akhavan, S.; Hadavi, R. Nano-encapsulation of fish oil in nano-liposomes and its application in fortification of yogurt. *Food Chem.* **2017**, *216*, 146−152.
(33) Kakavas, S.; Kotsiou, O. S.; Perlikos, F.; Mermiri, M.; Mavrovounis, G.; Gourgoulianis, K.; Pantazopoulos, I. Pulmonary function testing in COPD: looking beyond the curtain of FEV1. *NPJ Prim. Care Resp. M.* **2021**, *31*, 23.
(34) Lewis, K. L.; Helgeson, S. A.; Tatari, M. M.; Mallea, J. M.; Baig, H. Z.; Patel, N. M. COVID-19 and the effects on pulmonary function following infection: A retrospective analysis. *eClinicalMedicine* **2021**, *39*, No. 101079.
(35) Zhao, X.; Qiao, D.; Yang, C.; Kasela, S.; Kim, W.; Ma, Y.; Shrine, N.; Batini, C.; Sofer, T.; Taliun, S. A. G.; Sakornsakolpat, P.; Balte, P. P.; Prokopenko, D.; Yu, B.; Lange, L. A.; Dupuis, J.; Cade, B. E.; Lee, J.; Gharib, S. A.; Daya, M.; Laurie, C. A.; Ruczinski, I.; Cupples, L. A.; Loehr, L. R.; Bartz, T. M.; Morrison, A. C.; Psaty, B. M.; Vasan, R. S.; Wilson, J. G.; Taylor, K. D.; Durda, P.; Johnson, W. C.; Cornell, E.; Guo, X.; Liu, Y.; Tracy, R. P.; Ardlie, K. G.; Aguet, F.; VanDenBerg, D. J.; Papanicolaou, G. J.; Rotter, J. I.; Barnes, K. C.; Jain, D.; Nickerson, D. A.; Muzny, D. M.; Metcalf, G. A.; Doddapaneni, H.; Dugan-Perez, S.; Gupta, N.; Gabriel, S.; Rich, S. S.; O'Connor, G. T.; Redline, S.; Reed, R. M.; Laurie, C. C.; Daviglus, M. L.; Preudhomme, L. K.; Burkart, K. M.; Kaplan, R. C.; Wain, L. V.; Tobin, M. D.; London, S. J.; Lappalainen, T.; Oelsner, E. C.; Abecasis, G. R.; Silverman, E. K.; Barr, R. G.; Cho, M. H.; Manichaikul, A.; NHLBI, T. F. P. M.; TOPMed, L. W. G. Whole genome sequence analysis of pulmonary function and COPD in 19,996 multi-ethnic participants. *Nat. Commun.* **2020**, *11*, 5182.
(36) Agasing, A. M.; Wu, Q.; Khatri, B.; Borisow, N.; Ruprecht, K.; Brandt, A. U.; Gawde, S.; Kumar, G.; Quinn, J. L.; Ko, R. M.; Mao-Draayer, Y.; Lessard, C. J.; Paul, F.; Axtell, R. C. Transcriptomics and proteomics reveal a cooperation between interferon and T-helper 17 cells in neuromyelitis optica. *Nat. Commun.* **2020**, *11*, 2856.
(37) Li, J.; Wang, X.; Mei, K.; Chang, C. H.; Jiang, J.; Liu, X.; Liu, Q.; Guiney, L. M.; Hersam, M. C.; Liao, Y.; Meng, H.; Xia, T. Lateral size of graphene oxide determines differential cellular uptake and cell death pathways in Kupffer cells, LSECs, and hepatocytes. *Nano today* **2021**, *37*, No. 101061.
(38) Cutler, R. G.; Kelly, J.; Storie, K.; Pedersen, W. A.; Tammara, A.; Hatanpaa, K.; Troncoso, J. C.; Mattson, M. P. Involvement of oxidative stress-induced abnormalities in ceramide and cholesterol metabolism in brain aging and Alzheimer's disease. *Proc. Natl. Acad. Sci. U. S. A.* **2004**, *101*, 2070−2075.
(39) Reynolds, C. P.; Maurer, B. J.; Kolesnick, R. N. Ceramide synthesis and metabolism as a target for cancer therapy. *Cancer Lett.* **2004**, *206*, 169−180.
(40) Olivera, A.; Spiegel, S. Sphingosine-1-phosphate as second messenger in cell proliferation induced by PDGF and FCS mitogens. *Nature* **1993**, *365*, 557−560.
(41) Sharma, V.; McNeill, J. H. To scale or not to scale: the principles of dose extrapolation. *Br. J. Pharmacol.* **2009**, *157*, 907−921.
(42) Liu, X.; Meng, H. Consideration for the scale-up manufacture of nanotherapeutics-A critical step for technology transfer. *View* **2021**, *2*, No. 20200190.
(43) Serhan, C. N. Pro-resolving Lipid Mediators Are Leads for Resolution Physiology. *Nature* **2014**, *510*, 92−101.
(44) Serhan, C. N.; Levy, B. D. Resolvins in Inflammation: Emergence of the Pro-Resolving Superfamily of Mediators. *J. Clin. Investig.* **2018**, *128*, 2657−2669.
(45) Xu, L.; Yang, Y.; Simien, J. M.; Kang, C.; Li, G.; Xu, X.; Haglund, E.; Sun, R.; Zuo, Y. Y. Menthol in electronic cigarettes causes biophysical inhibition of pulmonary surfactant. *Am. J. Physiol. Lung Cell Mol. Physiol.* **2022**, *323*, L165−L177.
(46) Wang, P.; Nie, X.; Wang, Y.; Li, Y.; Ge, C.; Zhang, L.; Wang, L.; Bai, R.; Chen, Z.; Zhao, Y.; Chen, C. Multiwall carbon nanotubes mediate macrophage activation and promote pulmonary fibrosis through TGF-β/Smad signaling pathway. *Small* **2013**, *9*, 3799−3811.
(47) Fredman, G.; Hellmann, J.; Proto, J. D.; Kuriakose, G.; Colas, R. A.; Dorweiler, B.; Connolly, E. S.; Solomon, R.; Jones, D. M.; Heyer, E. J.; Spite, M.; Tabas, I. An imbalance between specialized pro-resolving lipid mediators and pro-inflammatory leukotrienes promotes instability of atherosclerotic plaques. *Nat. Commun.* **2016**, *7*, 12859.
(48) Zhang, L.; Terrando, N.; Xu, Z.; Bang, S.; Jordt, S.; Maixner, W.; Serhan, C. N.; Ji, R. Distinct analgesic actions of DHA and DHA-derived specialized pro-resolving mediators on post-operative pain after bone fracture in mice. *Front. Pharmacol.* **2018**, *9*, 412.
(49) Bakry, A. M.; Abbas, S.; Ali, B.; Majeed, H.; Abouelwafa, M. Y.; Mousa, A.; Liang, L. Microencapsulation of oils: A comprehensive review of benefits, techniques, and applications. *Compr. Rev. Food Sci. F.* **2016**, *15*, 143−182.
(50) Stewart, J. C. M. Colorimetric determination of phospholipids with ammonium ferrothiocyanate. *Anal. Biochem.* **1980**, *104*, 10−14.

https://doi.org/10.1021/acsnano.2c10388
ACS Nano XXXX, XXX, XXX−XXX